

Polarization direction and stability in ferroelectric lead titanate thin films

Ø. Dahl,^{a)} J. K. Grepstad, and T. Tybell^{b)}

Department of Electronics and Telecommunications, Norwegian University of Science and Technology, O.S. Bragstads Plass 2a, NO-7491 Trondheim, Norway

(Received 3 July 2009; accepted 6 September 2009; published online 26 October 2009)

In this article, we examine the initial polarization of PbTiO₃ thin films grown epitaxially on SrRuO₃ electrodes. It is found that the as-grown predominant polarization is directed toward the SrRuO₃ bottom electrode in films thinner than 20 nm and directed toward the top surface in thicker films. The data is interpreted in terms of a Landau–Ginzburg–Devonshire model for a semiconducting ferroelectric with asymmetric boundary conditions. Based on the measured hysteresis loops and the stability of the two polarization directions with time, it is concluded that charged defects serve to impose a preferential downward polarization in very thin films. © 2009 American Institute of Physics. [doi:10.1063/1.3240331]

I. INTRODUCTION

Ferroelectric thin films for device applications are often polarized perpendicular to the film surface. Ideally, the polarization is compensated by screening charges in short-circuited electrodes. When such boundary conditions are not satisfied, stable polarization can be explained by internal screening in a Landau–Ginzburg–Devonshire model.^{1–3} As was shown by Guro *et al.*,² the contact potential of the ferroelectric–electrode interface affects the polarization in the ferroelectric. Hence ferroelectric thin film structures with only one electrode may exhibit a preferred direction of polarization, which is often observed experimentally. For example, ferroelectric PbTiO₃ thin films grown on Nb-doped SrTiO₃ electrodes were found to be monodomain with positive polarization (i.e., \vec{P} directed toward the substrate),⁴ while similar films grown on SrRuO₃ electrodes have shown negative polarization.⁵ Monodomain films with positive polarization as well as polydomain films with periodically alternating positive and negative domains have been reported for PbTiO₃ grown on insulating SrTiO₃ substrate.^{6–8} In addition to the substrate material, the size of the ferroelectric material has also been found to affect the initial polarization. Inversion of the net polarization upon increasing size was observed for PbTiO₃ particles deposited on Nb-doped SrTiO₃ substrate, from positive polarization in small particles to negative polarization for particles larger than $\sim 10^5$ nm³.⁹ A similar effect was observed for PbTiO₃ thin films grown on La_{0.67}Sr_{0.33}MnO₃ electrodes, which changed from a polydomain to a monodomain state with negative polarization when the film thickness exceeded 25 nm.¹⁰ It has also been found that the oxygen pressure under high temperature processing can be used to reversibly switch the polarization in PbTiO₃ films with a SrRuO₃ bottom electrode.¹¹ At the moment, it is not established to what extent the polarization is screened by domain formation, external, or internal charges.

Here, we investigate the initial polarization and the stability of the switched polarization in PbTiO₃ thin films grown on SrRuO₃ electrodes. We use a Landau–Ginzburg–Devonshire model for an ideal semiconducting ferroelectric to theoretically assess the initial polarization, extending the symmetric models of Ivanchik,¹ Guro *et al.*,² Chenskii,⁵ and Watanabe,¹² with boundary conditions appropriate for a thin film with a vacuum interface on one side and a metallic electrode on the other.

II. EXPERIMENTAL

PbTiO₃ films with a thickness ranging from 5 to 100 nm were grown on SrRuO₃ epilayers deposited on SrTiO₃ substrate. The films were grown by off-axis rf magnetron sputtering from a Pb_{1.1}TiO₃ target in an O₂:Ar (4:10) atmosphere with a total pressure of 165 mTorr at a growth temperature of 540 °C. The films were *c*-axis oriented, with a mosaic spread of $<0.03^\circ$, as measured by x-ray diffraction rocking curves around the (001) and (002) reflections. The step-and-terrace surface topography of the substrates was replicated for films thinner than 100 nm, while thicker films had a root-mean-square surface roughness of less than 0.4 nm. Further details on film deposition and crystalline structure characterization are reported elsewhere.¹³ The SrRuO₃ layer was used as bottom electrode and 0.12 mm² Au/Pt contacts (200/50 nm thick) deposited *ex situ* were used as top electrodes for electrical characterization.

Polarization hysteresis curves were measured with a conventional Sawyer–Tower type setup (Aixacct TF2000). Asymmetric triangular bipolar voltage pulses were used, as reported previously,¹³ and the measurement frequency was 1 kHz. Pyroelectric hysteresis curves were measured as described by Chynoweth.¹⁴ The samples were locally heated using a 40 mW laser of 830 nm wavelength focused on the top electrode. The laser beam was pulsed using a mechanical chopper, and the resulting pyroelectric current was detected with a phase-locked amplifier. A current-to-voltage converter was used to ensure short-circuit conditions during measurements. The samples were polarized by voltage pulses with a pulse length of 1 s. The dwell time between polarization and

^{a)}Present address: SINTEF Materials and Chemistry, NO-7465 Trondheim, Norway. Electronic mail: oystein.dahl@sintef.no.

^{b)}Electronic mail: thomas.tybell@iet.ntnu.no.

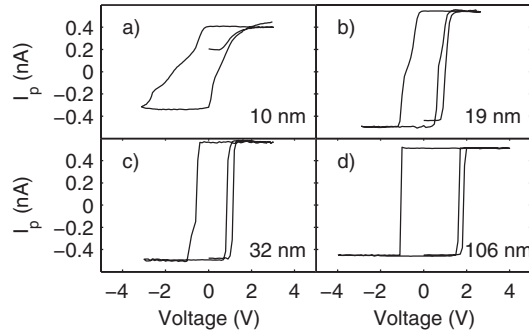


FIG. 1. Pyroelectric hysteresis loops measured on as-grown PbTiO₃ films. The initial response is positive in the 10 nm thick sample (a), while it is negative in the thicker samples [(b)–(d)].

measurement of the pyroelectric response was 5 s. Hysteresis loops were mapped out by applying a sequence of pulses with increasing and decreasing voltage amplitude. The stability of the polarization was examined by monitoring the time response of the pyroelectric current after forced polarization. The samples remained short-circuited throughout these measurements.

III. RESULTS AND DISCUSSION

The initial pyroelectric hysteresis loops, measured during the first switching of polarization, are shown in Fig. 1. The 10 nm thick film, Fig. 1(a), showed a positive initial pyroelectric response, while thicker films such as the 19 nm thick film, Fig. 1(b), showed a negative initial response. Films thicker than ~30 nm, Figs. 1(c) and 1(d), showed a negative initial response close to saturation. The response of a 5 nm thick film was consistent with a positive polarization; however, this film could not be switched in the present experiment. The PbTiO₃ samples in this study showed a change in net polarization with film thickness, with a positive initial polarization for the thinnest films, thus differing from previous reports, which found a negative polarization for all film thicknesses.⁵ Polarization hysteresis loops are shown in Fig. 2. Leakage current in samples thinner than ~20 nm made polarization measurements by the conventional technique unreliable. The polarization data show a similar trend as the pyroelectric loops, with a less sharp switching voltage for the thinnest samples. This is also evident from the current-voltage data shown by broken curves in Fig. 2.

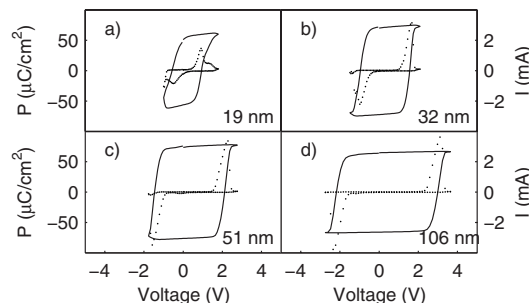


FIG. 2. Polarization hysteresis loops measured on PbTiO₃ films. The solid curves are the measured polarization (left ordinate axis) and the broken curves the measured current (right ordinate axis).

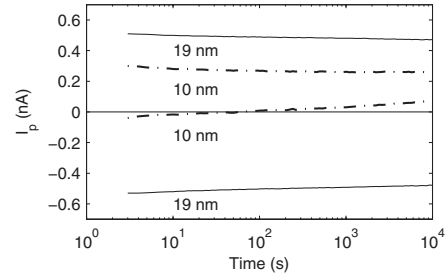


FIG. 3. The measured pyroelectric response vs time after polarization for two film thicknesses, 19 nm (solid curves) and 10 nm (dashed curves). The 10 nm thick film reverts to a net positive polarization after being switched to a negative state. For thicker films the response is symmetric.

The stability of the switched polarization with time is shown in Fig. 3 for a 10 nm and a 19 nm thick film, respectively. The pyroelectric response was found to decline nearly logarithmic with time after polarization. Thick films showed no measurable difference in stability between the two polarization states. Only for very thin films, initially polarized in the positive state, is an asymmetry of the polarization state clearly observed. After the film is negatively polarized, it reverts to a positive polarization.

The predominantly negative initial polarization has been previously attributed to polarization screening by negative ions in the growth chamber.⁵ Here, the influence of the electrode configuration on the polarization direction is examined. In a perfectly insulating ferroelectric, the electric field associated with the polarization gradient tends to destabilize the polarization. In a semiconducting ferroelectric, the surface band-bending can induce a screening charge to stabilize the polarization.^{1–3}

Following Ivanchik¹ and Guro *et al.*,² the Landau–Ginzburg–Devonshire expansion of the elastic Gibbs free energy density in the ferroelectric material in terms of the displacement field D ,

$$G = G_0 + \frac{K}{2} \left(\frac{dD}{dz} \right)^2 + \frac{A(T)}{2} D^2 + \frac{B}{4} D^4 + \frac{C}{6} D^6, \quad (1)$$

is used to find the equation of state relating the electric field E and the displacement D . The elastic energy is incorporated by rescaling the thermodynamic constants A and B .^{15,16} The effect of the bottom electrode interface and the film surface is included through the boundary conditions and the energy associated with the gradient of the displacement field near the film surface. The thermodynamic constants A , B , and C are known experimentally for PbTiO₃,¹⁷ and Zhirnov's estimate for the constant K ,¹⁵ assuming that the polarization varies over distances on the order of a lattice constant a_0 , is adopted by setting $K = A(0)a_0^2$.¹⁸ The displacement field profile and the charge density are found self-consistently from the equation of state, which gives the electric field as the variational derivative of the elastic Gibbs free energy density,

$$E = \frac{\partial G}{\partial D} - \frac{d}{dz} \left(\frac{\partial G}{\partial \frac{dD}{dz}} \right) = -K \frac{d^2 D}{dz^2} + AD + BD^3 + CD^5. \quad (2)$$

The electric field is by definition equal to the negative of the gradient of the electrostatic potential ϕ . Thus,

$$AD + BD^3 + CD^5 = K \frac{d^2 D}{dz^2} - \frac{d\phi}{dz}, \quad (3)$$

which by multiplication with the charge density $\rho = dD/dz$ gives

$$(AD + BD^3 + CD^5)dD = \left(K - \frac{d\phi}{d\rho} \right) \rho d\rho. \quad (4)$$

Integrating (4) over the PbTiO₃ layer gives

$$\left[\frac{A}{2} D^2 + \frac{B}{4} D^4 + \frac{C}{6} D^6 \right]_{D(z_1)}^{D(z_2)} = \frac{K}{2} [\rho^2]_{\rho(z_1)}^{\rho(z_2)} - [\rho\phi]_{\rho(z_1)}^{\rho(z_2)} + \int_{\rho(z_1)}^{\rho(z_2)} \phi d\rho, \quad (5)$$

where the solution of the final integral depends on the relation between charge density and electrostatic potential. For a semiconductor, the charge density is

$$\rho = q[p - n + N_d^+ - N_a^-], \quad (6)$$

where q is the electron charge, n and p are the electron and hole densities, and $q(N_d^+ - N_a^-)$ the net charge density from the dopants. For an intrinsic semiconductor, the Boltzmann approximation gives $\rho(\phi) = 2qn_i \sinh(-\beta\phi)$,¹⁹ where n_i is the intrinsic carrier density.²⁰ The potential ϕ is measured relative to the chemical potential of the neutral semiconductor and $\beta = q/kT$, where k is Boltzmann's constant and T the absolute temperature. The numerical calculations show that the induced charge density at the surface invalidates the Boltzmann approximation. Therefore, Joyce and Dixon's approximation for the relation between the reduced electrochemical potential $\eta_n = (\mu + q\phi - E_c)/kT$ and the electron density n ,²¹

$$\eta_n = \ln\left(\frac{n}{N_c}\right) + \sum_{m=1} A_m \left(\frac{n}{N_c}\right)^m, \quad (7)$$

is used instead of the Boltzmann approximation. Here μ is the chemical potential, E_c is the conduction band edge, and N_c is the conduction band effective density of states. Joyce and Dixon derive the coefficients A_m from a reversion of the power series expansion of the Fermi integral in terms of $\exp(\eta)$.²¹ The same approximation is used for the hole density p , with the reduced electrochemical potential replaced by $\eta_p = (E_v - \mu - q\phi)/kT$, where E_v is the valence band edge. N_c is replaced by the valence band effective density of states P_v . In the numerical calculations, the approximation is limited to the first four terms.²² Setting $d\rho = q(dp - dn)$, the integral in Eq. (5) is written

$$\int_{\rho(z_1)}^{\rho(z_2)} \phi(\rho) d\rho = q \int_{\rho(z_1)}^{\rho(z_2)} \phi(\eta_p) dp - q \int_{n(z_1)}^{n(z_2)} \phi(\eta_n) dn. \quad (8)$$

From Eq. (7), relating ϕ and n ,

$$\begin{aligned} -q \int \phi dn &= - \int \left\{ kT \left[\ln\left(\frac{n}{N_c}\right) + \sum_m A_m \left(\frac{n}{N_c}\right)^m \right] \right. \\ &\quad \left. + (\mu - E_c) \right\} dn \\ &= -n \left\{ kT \left[\ln\left(\frac{n}{N_c}\right) - 1 + \sum_m \frac{A_m}{m+1} \left(\frac{n}{N_c}\right)^m \right] \right. \\ &\quad \left. + (\mu - E_c) \right\}, \end{aligned} \quad (9)$$

with a corresponding expression for the integral over the hole density. For the numerical calculations, the minority carrier density was estimated from the law of mass action, $(n, p) = n_i^2 / (p, n)$. The majority carrier density was found from Eq. (6).

The PbTiO₃/SrRuO₃ system is modeled as an ideal semiconducting monodomain ferroelectric with a free electron gas bottom electrode. For this asymmetric configuration, the boundary condition at the surface is

$$D = 0, \quad (10)$$

and the displacement field and potential at the ferroelectric-metal interface are related by

$$\phi = \frac{\lambda}{\epsilon_r \epsilon_0} D - \Delta\Phi, \quad (11)$$

where $\Delta\Phi$ is the contact potential, and λ and ϵ_r are the screening length and the relative dielectric constant of the metallic electrode, respectively.²³ The displacement field will increase from zero at the film surface to an extreme value D_0 , either in the interior of the film or at the ferroelectric-metal interface. If the extreme is found in the interior of the film, it follows that the gradient of the displacement field is zero there. Hence, there is a neutral plane where $\rho = 0$ and $\phi = 0$. Equation (5) can then be solved numerically for D in terms of ϕ . If no neutral plane is found, Eq. (5) can be solved with $D = D_0$ at the ferroelectric-metal interface and ϕ given by Eq. (11). The displacement field profile and corresponding film thickness were found by numerical integration of the inverse charge density over the displacement field, from the film surface to the film-bottom electrode interface.

In Fig. 4, the solid line shows the magnitude of D_0 versus the film thickness for an intrinsic semiconducting ferroelectric with contact potential $\Delta\Phi = -0.3$ V and negative polarization. The contact potential was set equal to $\Phi_m - (\chi_s + V_n)$, where $q\Phi_m$ is the work function of the metal electrode, and $q\chi_s$ and qV_n are the electron affinity and the difference between the conduction band minimum and the chemical potential, respectively.²⁴ The reported literature values are $\Phi_m = 4.9$ V for SrRuO₃ and $\chi_s = 3.5$ V for PbTiO₃.^{25,26} While some uncertainty is involved in the assessment of the exact value of the chemical potential, equal effective density of states is assumed for the conduction and the valence band,

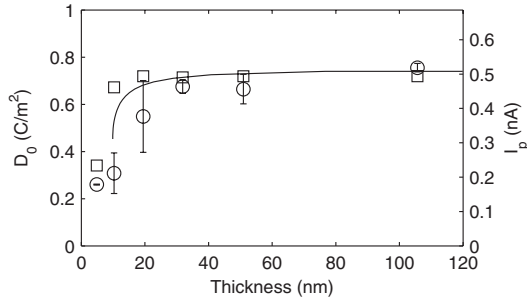


FIG. 4. The relationship between film thickness and displacement field, as obtained from a Landau–Ginzburg–Devonshire model at room temperature (solid line). The open circles mark the experimental initial pyroelectric response (right ordinate axis) and the open squares shows the displacement field calculated from the measured lattice constant (left ordinate axis).

and $V_n = E_g/2q$, with $E_g = 3.4$ eV for PbTiO_3 .²⁶ As can be seen, for a film thickness of less than 10 nm, the model has no solution for the displacement field. For films thicker than 10 nm, there is a finite solution for the displacement field, which increases with thickness and saturates for films thicker than 40 nm. Considering only the asymmetry arising from the contact potential at the film–bottom electrode interface, the negative polarization state is about 0.1 J/m^2 lower in energy than the positive polarization state for any film thickness. The free energy density in the infinitely thick film limit is about $1 \times 10^8 \text{ J/m}^3$ lower than the paraelectric reference structure. Thus for a 10 nm thick film, the energy difference between positive and negative polarization amounts to about 10% of the total change in free energy.

Figure 4 also shows experimental data for the magnitude of the initial pyroelectric response (open circles). The measured pyroelectric response is seen to increase less rapidly with increasing film thickness than predicted by the model. The measured pyroelectric response is a surface average over both positive and negative domains. Hence, for thin films where the depolarization field is stronger, resulting in a more even distribution of positive and negative domains, the net response is less than predicted for a monodomain thin film.

It is also possible to relate the polarization to the unit cell tetragonality. From the elastic Gibbs free energy,¹⁷ under the appropriate mechanical boundary conditions,¹⁶ the relation between the out-of plane lattice constant c and the displacement field D reads

$$D^2 = \frac{1}{Q_{11} - \frac{2s_{12}}{s_{11} + s_{12}} Q_{12}} \left[\frac{c}{a_0} - \left(1 + \frac{2s_{12}}{s_{11} + s_{12}} u_0 \right) \right], \quad (12)$$

where a_0 is the cubic lattice constant, u_0 is the in-plane strain imposed by the epitaxial growth on the SrTiO_3 substrate, s_{11} and s_{22} are the elastic compliance coefficients, and Q_{11} and Q_{12} are the electrostrictive constants. The displacement field calculated from Eq. (12) with the measured lattice constant c ,¹³ using values for the electrostrictive coefficients and the cubic lattice constant as given by Haun *et al.*,¹⁷ and elastic compliance coefficients taken from Ref. 27, is shown as open squares in Fig. 4. The calculated displacement field from the measured lattice constant is in good agreement with the predictions from the model and increases more rapidly than the

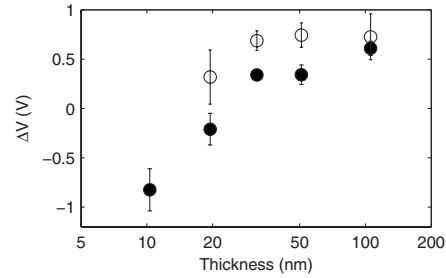


FIG. 5. The measured offset voltage of the pyroelectric (filled circles) and ferroelectric (open circles) hysteresis loops. The voltage offset is negative in thin films, going positive and increasing with film thickness to saturate at ~ 0.5 V.

pyroelectric response, again indicating the effect of domain formation for very thin films.

The observed change in stable polarization direction is not predicted by the present model for an intrinsic semiconductor, for which negative polarization is stable for all film thicknesses. We note that if the chemical potential changes as a result of doping, this will have two potentially opposing effects. (i) The contact potential will change. A net donor doping reduces V_n and makes the contact potential less negative or even positive, potentially stabilizing the positive polarization direction. Whereas a net acceptor doping may help stabilize the negative polarization direction. (ii) The amount of surface band bending required to induce a sufficient screening charge is changed. A net donor doping decreases the screening energy at the surface for the negative polarization direction, while a net acceptor doping decreases the energy for a positive polarization direction. Calculations with net acceptor dopant densities from 10^{-1} to 10^9 cm^{-3} gave lowest energy for positive polarization in thin films and for negative polarization in thick films, with a crossover thickness in the range of 20–30 nm.

The above analysis does not include the influence of defects. Internal fields can result from charged defects and defect dipoles.^{28–33} In Fig. 5, the voltage offset, defined as half the sum of the coercive switching voltages for positive and negative polarization, are shown for pyroelectric (filled circles) and polarization (open circles) hysteresis measurements. The offset voltage for thick films (>30 nm) corresponds to the built-in offset expected from the difference in work function for the Pt and SrRuO_3 electrodes. For thinner films the offset voltage decreases and reaches -0.8 V for the 10 nm thick film. Polarization hysteresis loops from 20 nm thick films grown at different temperatures¹³ showed an increasing negative voltage offset for films grown at the highest temperatures. Combined with the spontaneous switching to positive polarization, this suggests an increased influence from defects in the thinnest films. The preferred positive polarization and negative offset voltage in thin films are compatible with positively charged oxygen vacancies at the surface. Additional mechanisms are needed to explain the change in preferred polarization direction with increasing film thickness. A realistic model of the interaction and the dynamics between defects and the polarization during film growth would be valuable in order to understand the real thin film behavior.

IV. CONCLUSION

In summary, calculations on an idealized model indicate that the as-grown state of the PbTiO₃ films will have a preference for one of the two opposite polarization directions, depending on the contact potential between the ferroelectric thin film and the metal bottom electrode. Very thin films show voltage offsets and retention behavior compatible with a layer of positive charge near the top electrode.

ACKNOWLEDGMENTS

The authors acknowledge support from the Research Council of Norway under Grant No. 162874/V00. Professor Asle Sudbø is acknowledged for scientific discussions.

- ¹I. I. Ivanchik, *Sov. Phys. Solid State* **3**, 2705 (1962).
- ²G. M. Guro, I. I. Ivanchik, and N. F. Kovtonyuk, *Sov. Phys. Solid State* **11**, 1574 (1970).
- ³E. V. Chenskii, *Sov. Phys. Solid State* **12**, 446 (1970).
- ⁴C. Lichtensteiger, J.-M. Triscone, J. Junquera, and P. Ghosez, *Phys. Rev. Lett.* **94**, 047603 (2005).
- ⁵D. D. Fong, A. M. Kolpak, J. A. Eastman, S. K. Streiffer, P. H. Fuoss, G. B. Stephenson, C. Thompson, D. M. Kim, K. J. Choi, C. B. Eom, I. Grinberg, and A. M. Rappe, *Phys. Rev. Lett.* **96**, 127601 (2006).
- ⁶C. Thompson, C. M. Foster, J. A. Eastman, and G. B. Stephenson, *Appl. Phys. Lett.* **71**, 3516 (1997).
- ⁷S. K. Streiffer, J. A. Eastman, D. D. Fong, C. Thompson, A. Munkholm, M. V. Ramana Murty, O. Auciello, G. R. Bai, and G. B. Stephenson, *Phys. Rev. Lett.* **89**, 067601 (2002).
- ⁸R. Takahashi, J. K. Grepstad, T. Tybell, and Y. Matsumoto, *Appl. Phys. Lett.* **92**, 112901 (2008).
- ⁹S. H. Ahn, W. W. Jung, and S. K. Choi, *Appl. Phys. Lett.* **86**, 172901 (2005).
- ¹⁰C. Lichtensteiger, M. Dawber, N. Stucki, J.-M. Triscone, J. Hoffman, J.-B. Yau, C. H. Ahn, L. Despont, and P. Aebi, *Appl. Phys. Lett.* **90**, 052907 (2007).
- ¹¹R. V. Wang, D. D. Fong, F. Jiang, M. J. Highland, P. H. Fuoss, C. Thompson, A. M. Kolpak, J. A. Eastman, S. K. Streiffer, A. M. Rappe, and G. B. Stephenson, *Phys. Rev. Lett.* **102**, 047601 (2009).
- ¹²Y. Watanabe, *Phys. Rev. B* **57**, 789 (1998).
- ¹³Ø. Dahl, J. K. Grepstad, and T. Tybell, *J. Appl. Phys.* **103**, 114112 (2008).
- ¹⁴A. G. Chynoweth, *J. Appl. Phys.* **27**, 78 (1956).
- ¹⁵V. A. Zhirnov, *Sov. Phys. JETP* **8**, 822 (1959).
- ¹⁶N. A. Pertsev, A. G. Zembilgotov, and A. K. Tagantsev, *Phys. Rev. Lett.* **80**, 1988 (1998).
- ¹⁷M. J. Haun, E. Furman, S. J. Jang, H. A. McKinstry, and L. E. Cross, *J. Appl. Phys.* **62**, 3331 (1987).
- ¹⁸The calculations were performed assuming a temperature-independent strain, $u_{11}=u_{22}=u=-0.015$, with rescaled values for the thermodynamic constants according to Ref. 16, $A=A_0-u2Q_{12}/s_{11}+s_{12}$ and $B=B_0+Q_{12}^2/s_{11}+s_{12}$. The zero stress values were taken from Ref. 17: $A_0=\alpha(T-T_0)$ with $\alpha=7.530\times 10^5$ m/F K and $T_0=478.8$ °C, $B_0=-2.901\times 10^8$ m²/C² F, $C=1.5636\times 10^9$ m⁹/C⁴ F, $Q_{11}=8.9\times 10^{-2}$ m⁴/C², $Q_{12}=-2.6\times 10^{-2}$ m⁴/C², and K was estimated at 9.221×10^{-11} m³/F. $s_{11}=7.2\times 10^{-12}$ m³/C² F and $s_{12}=-2.1\times 10^{-12}$ m³/C² F were taken from Ref. 27.
- ¹⁹N. W. Ashcroft and N. D. Mermin, *Solid State Physics* (Harcourt College Publishers, Fort Worth, 1976).
- ²⁰The intrinsic equilibrium carrier density was estimated assuming a band gap of 3.4 eV and effective electron and hole masses of $10m_e$.
- ²¹W. B. Joyce and R. W. Dixon, *Appl. Phys. Lett.* **31**, 354 (1977).
- ²²For a parabolic band, the first four terms are $A_1\approx 3.53553\times 10^{-1}$, $A_2\approx -4.95009\times 10^{-3}$, $A_3\approx 1.48386\times 10^{-4}$, and $A_4\approx -4.42563\times 10^{-6}$. With these four terms, the expansion is accurate up to $\eta\approx 7$ (Ref. 21).
- ²³The screening length was set at 0.11 nm and the relative dielectric constant at 8.45 (Ref. 34).
- ²⁴S. M. Sze, *Physics of Semiconductor Devices*, 2nd ed. (Wiley, New York, 1981).
- ²⁵A. J. Hartmann, M. Neilson, R. N. Lamb, K. Watanabe, and J. F. Scott, *Appl. Phys. A: Mater. Sci. Process.* **70**, 239 (2000).
- ²⁶J. Robertson and C. W. Chen, *Appl. Phys. Lett.* **74**, 1168 (1999).
- ²⁷V. G. Gavrilachenko and E. G. Fesenko, *Sov. Phys. Crystallogr.* **16**, 549 (1971).
- ²⁸B. E. Deal, M. Sklar, A. S. Grove, and E. H. Snow, *J. Electrochem. Soc.* **114**, 266 (1967).
- ²⁹R. R. Mehta, B. D. Silverman, and J. T. Jacobs, *J. Appl. Phys.* **44**, 3379 (1973).
- ³⁰G. Arlt and H. Neumann, *Ferroelectrics* **87**, 109 (1988).
- ³¹G. E. Pike, W. L. Warren, D. Dimos, B. A. Tuttle, R. Ramesh, J. Lee, V. G. Keramidas, and J. T. Evans, Jr., *Appl. Phys. Lett.* **66**, 484 (1995).
- ³²M. Grossmann, O. Lohse, D. Bolten, U. Boettger, T. Schneller, and R. Waser, *J. Appl. Phys.* **92**, 2680 (2002).
- ³³A. K. Tagantsev, I. Stolichnov, N. Setter, and J. S. Cross, *J. Appl. Phys.* **96**, 6616 (2004).
- ³⁴D. J. Kim, J. Y. Jo, Y. S. Kim, Y. J. Chang, J. S. Lee, J.-G. Yoon, T. K. Song, and T. W. Noh, *Phys. Rev. Lett.* **95**, 237602 (2005).